RSC Advances

ROYAL SOCIETY OF CHEMISTRY

www.rsc.org/advances

Cite this: DOI: 10.1039/c0xx00000x

www.rsc.org/xxxxxx

ARTICLE TYPE

Synthesis, Crystal Structure and MMCT of New Cyanide-bridged Complexes *cis*-$M^{II}(dppm)_2(CN)_2(Fe^{III}X_3)_2$ (M = Ru，Os)

Yong Wang,[a, b] Jinshuai Song,[a] Xiao Ma,[a] Zhenzhen Xue,[a, b] Shengmin Hu,[a] Ruibiao Fu,[a] Chunsen Li,*[a, c] Tianlu Sheng*[a] and Xintao Wu[a]

Received (in XXX, XXX) Xth XXXXXXXXX 20XX, Accepted Xth XXXXXXXXX 20XX
DOI: 10.1039/b000000x

The syntheses, crystal structures, IR and electronic absorption spectroscopy of two cyanide precursors *cis*-$M^{II}(dppm)_2(CN)_2$ (M = Ru, **1**; Os, **2**) (dppm = bis(diphenylphosphino) methane) and four new cyanide-bridged complexes *cis*-$M^{II}(dppm)_2(CN)_2(Fe^{III}X_3)_2$ (M = Ru, X = Cl, **3**; M = Ru, X = Br, **4**; M = Os, X = Cl, **5**; M = Os, X = Br, **6**) are reported. The crystal structural data, IR and the MMCT (metal-to-metal charge transfer) in the electronic absorption spectroscopy indicate the existence of some electron delocalization along Fe^{III}-NC-M^{II} arrays in complexes **3-6**. The presence of a more new MMCT band of the Os-based complexes (**5** and **6**) than that of the Ru-based complexes (**3** and **4**) should result from the larger spin-orbit coupling (SOC) of Os^{II}. Also the theoretical calculated values of the crystal structural data and IR spectra are in good consistent with the experimental values. Temperature-dependent magnetic properties of complexes **3-6** reveal the presence of the very weak metal-metal interaction between distant Fe^{III} ions across the diamagnetic *cis*-$NCM^{II}(dppm)_2CN$- bridge.

Introduction

The electronic mixing between metal ions in mixed valence complexes can lead to delocalization of charge density, and this delocalization can alter the physical and chemical properties of the complexes.[1] Usually, it is difficult to obtain the extent of electronic delocalization between the metal centers. And the MMCT properties of the polynuclear complexes provide one of the most powerful and sensitive probes of degree of the metal-metal electronic interaction.[2, 3] Cyanide bridge is a good candidate to promote efficient mixing between the metal centres and opens the way for efficient electron and energy transfer, also the structures and physical properties between metal centres through the cyanide bridge can be controlled and predicted.[4] The myriad of applications in complexes take advantage of the versatile photophysical,[5] photochemical[6] and electrochemical[7] properties that are associated with the MMCT. A classic mixed valence cyanide-bridged example is Prussian blue, $Fe^{III}_4[Fe^{II}(CN)_6]$,[8] the intense blue attributed to light-induced electron transfer from the t_{2g} orbital of low-spin Fe^{II} ion to t_{2g} orbital of high-spin Fe^{III} ion through the cyanide bridge.

Hence it is significant to design and synthesis of polynuclear cyanide-bridged complexes with MMCT for investigating the electronic delocalization between metal ions. Recently, our group has reported the MMCT and metal-metal interaction of some polynuclear cyanide-bridged complexes.[9, 10] Herein, we report the synthesis, crystal structures, MMCT, magnetic properties and theoretical calculations of four cyanide-bridged heterobimetallic complexes *cis*-$[X_3Fe^{III}NCM^{II}(dppm)_2CNFe^{III}X_3]$ (M = Ru, X = Cl, **3**; M = Ru, X = Br, **4**; M = Os, X = Cl, **5**; M = Os, X = Br, **6**).

Experimental Methods

Physical Measurements

Elemental analyses (C, H, N) were carried out on a Vario MICRO elemental analyzer. Infrared (IR) spectra were recorded on a Vertex 70 FT-IR spectrophotometer using KBr pellets. Electronic absorption spectra were measured on a Perkin-Elmer Lambda 35 UV/vis spectrophotometer. The temperature-dependent magnetic susceptibilities of the polycrystalline samples were measured with a Magnetic Property Measurement System (MPMS) SQUID-XL under an applied magnetic field of 1000 Oe in a 2-300 K temperature range. Diamagnetic corrections for complexes **3-6** were made using Pascal's constants. Diamagnetic susceptibilities are -781.72×10^{-6} cm^3 K mol^{-1} for **3**, -848.92×10^{-6} cm^3 K mol^{-1} for **4**, -797.72×10^{-6} cm^3 K mol^{-1} for **5**, -864.92×10^{-6} cm^3 K mol^{-1} for **6**, respectively.

Materials and Syntheses

All the manipulations were performed under argon atmosphere with the use of standard Schlenk techniques unless otherwise stated. Dichloromethane was dried by distillation over calcium hydride and diethyl-ether was dried by distillation over sodium wire under argon atmosphere. Methanol was dried by distillation over magnesium and distilled water was used. *cis*-$Ru^{II}(dppm)_2Cl_2$[11-13] and *cis*-$Os^{II}(dppm)_2Cl_2$[11, 13] were prepared according to the literature procedures. All other

reagents were available commercially and used without further purification.

***cis*-$Ru^{II}(dppm)_2(CN)_2 \cdot CH_2Cl_2$, $1 \cdot CH_2Cl_2$.** Under argon atmosphere, a solution of *cis*-$Ru^{II}(dppm)_2Cl_2$ (940 mg, 1.0 mmol) in dichloromethane (50 ml) was mixed with KCN (1300 mg, 20 mmol) in H_2O (20 ml). The mixture was refluxed for 48 h, and then cooled to room temperature. The organic layer was separated and the aqueous residue was extracted with dichloromethane (3 × 20 ml). The combined organic extracts were dried over anhydrous $MgSO_4$, concentrated and dried in vacuum to give the desired product as a pale yellow solid (580 mg, 63%). The resultant residue was dissolved in a mixed solution of dichloromethane (10 ml), diethyl-ether (30 ml) and 2-propanol (1 ml), to give **1** as yellow crystals. Anal. Calc. for $RuC_{52}H_{44}P_4N_2 \cdot CH_2Cl_2$: C, 63.23; H, 4.60; N, 2.78%. Found: C, 63.51; H, 4.85; N, 2.79%. IR (KBr pellet, cm^{-1}): 2105 (CN), 2091 (CN). UV-vis (CH_3CN), λ_{max}, nm (ε, $dm^3\ mol^{-1}\ cm^{-1}$): 325 (2042), 361 (922).

***cis*-$Os^{II}(dppm)_2(CN)_2 \cdot CH_2Cl_2$, $2 \cdot CH_2Cl_2$.** This compound was synthesized from a mixed solution of *cis*-$Os^{II}(dppm)_2Cl_2$ (515 mg, 0.50 mmol) in 50 ml dichloromethane and KCN (650 mg, 10 mmol) in 20 ml H_2O using a similar procedure as described of **1**. The product was isolated as a pale yellow solid (258 mg, 51%). Anal. Calc. for $OsC_{52}H_{44}P_4N_2 \cdot CH_2Cl_2$: C, 58.08; H, 4.23; N, 2.56%. Found: C, 57.57; H, 4.39; N, 2.08%. IR (KBr pellet, cm^{-1}): 2108 (CN), 2088 (CN). UV-vis (CH_3CN), λ_{max}, nm (ε, $dm^3\ mol^{-1}\ cm^{-1}$): 318 (3213), 360 (824).

***cis*-$Ru^{II}(dppm)_2(CN)_2(Fe^{III}Cl_3)_2 \cdot C_3H_7OH$, $3 \cdot C_3H_7OH$.** Under argon atmosphere, a solution of *cis*-$Ru^{II}(dppm)_2(CN)_2$ (92.1 mg, 0.10 mmol) in dichloromethane (10 ml) was mixed with $Fe^{III}Cl_3$ (35.8 mg, 0.22 mmol) in MeOH (10 ml). The resulting solution was stirred at 35 °C for 3 h. The solvent was removed and dichloromethane (20 ml) was added to the resultant solid. The reaction mixture was filtered and the filtrate was concentrated under reduced pressure. The resultant residue was dissolved in a mixed solution of dichloromethane (10 ml), diethyl-ether (30 ml) and 2-propanol (1 ml) to give **3** as red crystals (87.5 mg, 67%). Anal. Calc. for $RuFe_2Cl_6C_{52}H_{44}P_4N_2$: C, 50.11; H, 3.56; N, 2.25%. Found: C, 49.48; H, 3.71; N, 2.31%. IR (KBr pellet, cm^{-1}): 2092 (CN), 2062 (CN). UV-vis (CH_3CN), λ_{max}, nm (ε, $dm^3\ mol^{-1}\ cm^{-1}$): 311 (12251), 358 (11229), 542 (2939).

***cis*-$Ru^{II}(dppm)_2(CN)_2(Fe^{III}Br_3)_2 \cdot 2CH_3OH$, $4 \cdot 2CH_3OH$.** The procedure described for complex **4** was similar to that of complex **3** by using *cis*-$Ru^{II}(dppm)_2(CN)_2$ (92.1 mg, 0.10 mmol) and $Fe^{III}Br_3$ (65.0 mg, 0.22 mmol). The product was obtained as brown crystals. Yield: (94.6 mg, 60%). Anal. Calc. for $RuFe_2Br_6C_{52}H_{44}P_4N_2 \cdot 2CH_3OH$: C, 41.13; H, 3.32; N, 1.78%. Found: C, 41.20; H, 3.10; N, 1.85%. IR (KBr pellet, cm^{-1}): 2090 (CN), 2058 (CN). UV-vis (CH_3CN), λ_{max}, nm (ε, $dm^3\ mol^{-1}\ cm^{-1}$): 390 (7551), 422 (7458), 464 (7128), 594 (2777).

***cis*-$Os^{II}(dppm)_2(CN)_2(Fe^{III}Cl_3)_2 \cdot CH_2Cl_2$, $5 \cdot CH_2Cl_2$.** The procedure described for complex **5** was similar to that of complex **3** by using *cis*-$Os^{II}(dppm)_2(CN)_2$ (101.0 mg, 0.10 mmol) and $Fe^{III}Cl_3$ (35.8 mg, 0.22 mmol). The product was obtained as red crystals. Yield: (72.4 mg, 51%). Anal. Calc. for $OsFe_2Cl_6C_{52}H_{44}P_4N_2 \cdot CH_2Cl_2$: C, 44.82; H, 3.26; N, 1.97%. Found: C, 45.04; H, 3.66; N, 1.90%. IR (KBr pellet, cm^{-1}): 2085 (CN), 2048(CN). UV-vis (CH_3CN), λ_{max}, nm (ε, $dm^3\ mol^{-1}\ cm^{-1}$): 301 (11914), 359 (10768), 542 (3996), 664 (2691).

***cis*-$Os^{II}(dppm)_2(CN)_2(Fe^{III}Br_3)_2$, 6.** The procedure described for complex **6** was similar to that of complex **3** by using *cis*-$Os^{II}(dppm)_2(CN)_2$ (101.0 mg, 0.10 mmol) and $Fe^{III}Br_3$ (65.0 mg, 0.22 mmol). The product was obtained as brown crystals. Yield: (91.3 mg, 57%). Anal. Calc. for $OsFe_2Br_6C_{52}H_{44}P_4N_2$: C, 38.98; H, 2.77; N, 1.75%. Found: C, 39.40; H, 2.92; N, 1.76%. IR (KBr pellet, cm^{-1}): 2081 (CN), 2042 (CN). UV-vis (CH_3CN), λ_{max}, nm (ε, $dm^3\ mol^{-1}\ cm^{-1}$): 390 (8322), 420 (8195), 466 (7534), 610 (2943), 740 (1984).

X-Ray Crystal Structure Determination

Single crystal X-ray crystallographic data of complexes **1-6** were collected on a Saturn724+ CCD diffractometer equipped with graphite-monochromatic Mo K_α (λ = 0.71073 Å) radiation using an ω scan mode at 123 K. The structure was solved by the direct methods with *SHELXL-97*[14] program and refined by full-matrix least-squares (*SHELXL- 97*) on F^2. Anisotropic thermal parameters were used for the non-hydrogen atoms, and isotropic parameters were used for the hydrogen atoms. Hydrogen atoms were added geometrically and refined using a riding model. The detail crystallographic data for **1-6** are summarized in Table 1. Selected bond lengths and angles for **1-6** are listed in Table 2.

CCDC-997326 (**1**), CCDC-997327 (**2**), CCDC-997328 (**3**), CCDC-997329 (**4**), CCDC-997330 (**5**), CCDC-997331 (**6**) contain the supplementary crystallographic data, related bond lengths and angles for this paper.

Computational Methods

Full geometry optimization and frequency calculation were carried out by unrestricted B3LYP functional[15] coupled with effective core potential plus double-basis set LANL2DZ on metal atoms and all-electron 6-31G** basis set on the other atoms using Gaussian 03 package.[16] The harmonic vibration frequencies were scaled by 0.9613 to fit the IR spectrum.[17] Energy correction and property calculations with larger basis set were performed by using ORCA program.[18] An all-electron basis set Def2-TZVP[19] was employed for all the atoms except Os for which the SDD pseudopotential basis set was used. The *g* tensor was computed at the same level.[20] Broken symmetry approach was used to calculate the effective exchange integrals (*J*) in Yamaguchi's formalism:[21]

$$J = ({}^{LS}E(X) - {}^{HS}E(X))/({}^{HS}\langle S^2\rangle(X) - {}^{LS}\langle S^2\rangle(X))$$

Results and Discussion

Synthesis

The pale-yellow precursors **1** and **2** were synthesized directly by refluxing of *cis*-$M^{II}(dppm)_2Cl_2$ (M = Ru, Os) in dichloromethane with extremely excess KCN (20 equiv.) in water for 2 days, respectively, which was different from the previous reports.[22] Recrystallization from CH_2Cl_2/Et_2O solution led to pale yellow crystals, which were characterized

by IR, electronic absorption spectra, elemental analysis and single-crystal X-ray diffraction analysis.

Complexes **3-6** were prepared in a straightforward way by reaction of *cis*-$M^{II}(dppm)_2(CN)_2$ (M = Ru, Os) in dichloromethane with 2 equivalents $Fe^{III}X_3$ (X = Cl, Br) in CH_3OH under ambient condition. By slow diffusion of diethyl-ether into the dichloromethane solution, red or brown crystals suitable for X-ray diffraction analysis were obtained. The obtained crystals were also characterized by electronic absorption spectra, IR, elemental analysis and X-ray diffraction, which agree with the formulation *cis*-$M^{II}(dppm)_2(CN)_2(Fe^{III}X_3)_2$.

Description of theCrystal Structures of 1–6

The precursors **1** and **2** are isostructural and their structural drawings are shown in Figure 1. Also, complexes **3-6** are isostrucural and their structural diagrams are shown in Figure 2. Compounds **1-6** all crystallize in triclinic space group *P*-1.

The molecular structures of complexes **1** and **2** consist of one mononuclear *cis*-$M^{II}(dppm)_2(CN)_2$ (M = Ru, **1**; M = Os, **2**) and an uncoordinated CH_2Cl_2 solvent molecule. The central Ru^{II} and Os^{II} ions in complexes **1** and **2** are six-coordinated by four phosphorus atoms from two bidentate dppm ligands and two carbon atoms from two cyanide groups in *cis*-position, giving a slightly distorted octahedron geometry. The backbones of complexes **3-6** adopt a V-shaped configuration with two FeX_3 moieties bridged by diamagnetic cyanidometal -NC-M^{II}-CN- bridge. The M^{II} centre is still in a distorted octahedral coordinated environment, which is similar to complexes **1** and **2**. The cyanide N-bonding Fe atoms show a tetrahedron coordination sphere linked with one nitrogen atom from cyanide group and three halogen atoms.

The bond lengths of C≡N vary a little from 1.141(4) and 1.152(5) Å for **1** to 1.137(6) and 1.143(6) Å for **2**. The M^{II}-C(CN) distances (2.035(4) and 2.045(3) Å) in **1** are shorter than those (2.058(4) and 2.060(4) Å) in **2** due to the larger radii of Os^{II} than Ru^{II}. The bond lengths of Ru^{II}-P1 (2.339(1) Å) and Ru^{II}-P3 (2.348(1) Å) are shorter than those of Ru^{II}-P2 (2.377(1) Å) and Ru^{II}-P4 (2.387(1) Å) in **1** owing to the structural *trans*-effect.[23] The bond lengths of Os^{II}-P1 (2.345 (1) Å) and Os^{II}-P3 (2.334 (1) Å) are shorter than those of Os^{II}-P2 (2.371 (1) Å) and Os^{II}-P4 (2.363 (1) Å) in **2**, which may also be due to the structural *trans*- effect.[23] The bond angles of N1≡C51-Ru^{II}1 and N2≡C52-Ru^{II}1 are 176.3(3)° and 175.0(3)° for **1** an 176.5(1)° and 177.0(3)° for **2**, and the angle of C52-M^{II}1-C51 are 84.6(1)° for **1** and 84.4(2)° for **2**.

In the Ru-based complexes (**1**, **3**, **4**), the bond distances of Ru^{II}-C in both **3** (1.988(7) and 1.992(7) Å) and **4** (1.975(7) and 1.983(7) Å) are shorter than those in **1** (2.035(4) and 2.045(3) Å) due to the electron-withdrawing effect of the Fe^{III} ions. The similar phenomenon can also be found in the Os-based complexes in which the distances of Os^{II}-C in both **5** (2.004(9) and 2.017(9) Å) and **6** (1.972(10) and 1.973(10) Å) are shorter than those in **2** (2.058(4) and 2.060(4) Å). The bond distances of M^{II}-C variation from the mononuclear precursors to the tri-nuclear complexes suggests the presence of a weak electron delocalization along Fe^{III}-NC-M^{II} arrays in **3 - 6**. This is also supported by the fact that there exist central $M^{II} \rightarrow$ terminal Fe^{III} MMCT in **3 – 6** (vide infra). The bond angles of N≡C-Ru in **3** are nearly linear with the angles of N1≡C51-Ru1 of 174.3(6)° and N2≡C52-Ru1 of 177.2(6)°. Unlike the angles of Ru–C≡N, the bond angles of Fe-N≡C(CN) in **3** deviate significantly from linearity with the angles of Fe1-N1≡C1 of 166.4(6)° and Fe2-N2≡C2 of 173.3(6)°, and the angle of C52-Ru1-C51 is 87.9(3)°. These similar behaviors can also be found in **4-6** in detail in Table 2.

The shortest intramolecular $Fe^{III}\cdots Ru^{II}$ distances in **3 - 6** are 5.0 ~ 5.1 Å, whereas the nearest $Fe^{III}\cdots Fe^{III}$ separations across the diamagnetic cyanidometal NC-M^{II}-CN bridge are about 10.2 Å for **3-6**.

IR Spectroscopy

The CN stretching vibrations (ν_{CN}) are extremely sensitive to the cyanide coordination to metal centres, thus ν_{CN} in the IR spectra can provide some useful formation about cyanide-bridged complexes. The IR data for the CN stretching frequencies for complexes **1-6** are listed in Table 3. There are two ν_{CN} IR bands for each complex (**1-6**) due to the combination of symmetric and asymmetric stretching frequencies in *cis*- configuration. In comparison to the related mononuclear cyanide precursors **1** and **2**, the ν_{CN} in complexes **3-6** is shifted to lower frequency. This is because the π back-bonding from the carbon-bound metal (Ru^{II} and Os^{II}) into the CN bond is enhanced when the cyanide is coordinated to the electron-attracting metal Fe^{III} ions, leading to a weakening of the C≡N bond and hence a shift to lower frequency for CN is expected.[24] From Table 3, both the experimental values and theoretical calculated values indicate the ν_{CN} stretching frequencies of the Ru-based complexes (**3** and **4**) are larger than that of the Os-based complexes (**5** and **6**). This should result from the stronger electron-donating property of Os^{II} than Ru^{II}. Also the separations between the two ν_{CN} bands of the Ru-based complexes (**3** and **4**) are smaller than that of the Os-based complexes (**5** and **6**).

Electronic Absorption Spectroscopy and MMCT

The electronic absorption spectra of the precursors **1** and **2** and complexes **3-6** were measured in the CH_3CN solution at room temperature and are shown in Figures 3 and 4, and the data are listed in Table 4. Complex **1** exhibits maximum absorption wavelengths at 325 nm and 361 nm, and complex **2** exhibits maximum absorption wavelengths at 318 nm and 360 nm in CH_3CN. According to the previous report,[11] these two low-intensity transitions bands of complexes **1** and **2** can be assigned to *d*-*d* transition ($t_{2g} \rightarrow e_g$) or MLCT (metal to ligand charge transfer) bands, corresponding to a signal from *d* orbital of metal to π^* orbital of the ligand.

The electronic absorption spectra of complexes **3** and **5** are shown in Figure 3. The formation of cyanide-bridged complex **3** is accompanied by the appearance of new bands at 311, 358 and 542 nm. The bands of 311 and 358 nm can also be assigned to MLCT bands, and the band at 542 nm should be assigned to MMCT (metal to metal charge transfer) due to the absence of the absorption band more than 500 nm of **1** and $FeCl_3$. The electronic absorption spectra of complex **5** is similar to that of complex **3**, but complex **5** has a more new band around 664 nm which may be predominantly split by SOC of diamagnetic Os^{II}.[2, 25] Such phenomenon was not observed in complex **3**,

this may be because the SOC of Ru^{II} is too weak.[26] The electronic absorption spectra of complexes **4** and **6** are similar to those of complexes **3** and **5**.

The degree of electronic delocalization depends on the energy and intensity of the MMCT band.[27] The lower the energy of MMCT band is, the smaller the energy gap between ground-state and charge transfer configurations is and thus a better electronic delocalization is. The energy and intensity of MMCT bands in **5** (542 nm (3996 dm^3 mol^{-1} cm^{-1})) is stronger than that of **3** (542 nm (2939 dm^3 mol^{-1} cm^{-1})), indicating the more degree of the electronic delocalization in the complex **5**. Also, the similar phenomenon can be seen in the Br-related complexes, the energy and intensity of MMCT bands of complex **6** (610 nm (2943 dm^3 mol^{-1} cm^{-1})) is stronger than that of **4** (594 nm (2777 dm^3 mol^{-1} cm^{-1})). From this phenomenon, it can be concluded that the electronic delocalization in the Os-based complexes (**5** and **6**) are better than that of the Ru-based complexes (**3** and **4**). This appearance can also be demonstrated by the related change of the Ru^{II}-C or Os^{II}-C bond distances (vide supra).

Magnetic Properties

To investigate whether there exists the metal-metal interaction between distant Fe^{III} ions across the diamagnetic *cis*-$NCM^{II}(dppm)_2CN$ bridge, magnetic properties of complexes **3-6** were measured and analysed. The variable-temperature magnetic susceptibilities of complexes **3-6** were performed on polycrystalline samples in the temperature range of 2-300 K under an external magnetic field of 1000 Oe (Figures 5-8). The $\chi_M T$ value of 8.67 cm^3 K mol^{-1} at 300 K for **3** is consistent with the spin-only value of 8.75 cm^3 K mol^{-1} expected for the two uncoupled HS Fe^{III} and one diamagnetic LS Ru^{II} ions (S_{Fe} = 5/2, S_{Ru}= 0, g = 2.0). While in the case of complex **5**, the $\chi_M T$ value of 7.27 cm^3 K mol^{-1} at 300 K is considerably lower than the spin-only value of 8.75 cm^3 K mol^{-1} expected for two isolated HS Fe^{III} and one diamagnetic LS Os^{II} ions (S_{Fe} = 5/2, S_{Os}= 0, g = 2.0). The $\chi_M T$ values of **3** and **5** keep almost constant until 50 K, then both of them exhibit an abrupt decrease down to 7.88 and 6.63 cm^3 K mol^{-1} at 2 K for **3** and **5**, respectively. The magnetic properties of **3** and **5** were fitted by the Curie-Weiss law, $\chi_M = C/(T - \theta)$. The values of the best fitting for all experiment points leading to C = 8.66 cm^3 K mol^{-1} and θ = -0.18 K for **3** , and C = 6.96 cm^3 K mol^{-1} and θ = -0.12 K for **5**. These magnetic behaviors indicate weak anti-ferromagnetic coupling in complexes **3** and **5** between paramagnetic Fe^{III} ions across the diamagnetic cyanidometal bridge.

In the case of complexes **4** and **6**, the $\chi_M T$ value of 8.79 cm^3 K mol^{-1} at 300 K for **4** is very close to the spin-only value 8.75 cm^3 K mol^{-1} expected for two uncoupled HS Fe^{III} and one diamagnetic LS Ru^{II} ions (S_{Fe} = 5/2, S_{Ru}= 0, g = 2.0). Whereas in the case of complex **6**, the observed $\chi_M T$ value of 8.09 cm^3 K mol^{-1} at 300 K is considerably lower than the spin-only value 8.75 cm^3 K mol^{-1} for two uncoupled HS Fe^{III} and one diamagnetic LS Os^{II} ions (S_{Fe} = 5/2, S_{Os}= 0, g = 2.0). Upon lowering the temperature, the value of $\chi_M T$ for **4** and **6** keep almost constant until 14 K, then sharply decrease to 6.96 and 5.94 cm^3 K mol^{-1} at 2 K for **4** and **6**, respectively. The plot of χ_M versus T in the whole temperature range obey Curie-Weiss law, $\chi_M = C/(T - \theta)$, with C = 8.77 cm^3 K mol^{-1}, θ = -0.05 K for **4** and C = 8.12 cm^3 K mol^{-1}, θ = -1.16 K for **6**. The negative Weiss values indicate the presence of weak anti-ferromagnetic interaction for complexes **4** and **6** between paramagnetic Fe^{III} ions across the diamagnetic cyanidometal bridge.

By comparison with the magnetic properties of the cyanide-bridged complexes reported by us,[9] the magnetic interaction between paramagnetic Fe^{III} ions across the diamagnetic cyanidometal bridge is very weak in complexes **3-6**, which was supported by theoretical calculations as follows.

Theoretical Calculations

Table S1 collects the B3LYP optimized geometric data of species **1-6** and wherever possible compares them to crystal structures. It is seen that the computed data is in reasonable accord with experiment. The differences between theoretical and experimental bond lengths of M-C, Fe-N, Fe-X and C≡N are less than 0.06 Å except that the computed M-P bonds are slightly longer than the corresponding crystal bonds due to the weak-field effect by phosphorus atoms. Moreover, the optimized bond angles are in good agreement with the experimental data. Thus, our DFT calculations reproduce the experimental findings in the crystal structures of species **1-6**.

The relative energies of the possible spin-states (S = 0, 1, 2, 3, 4, 5) for complexes **3-6** are shown in Table 5. It is seen that all the compounds have a pair of degenerate spin-states, one singlet state (S = 0) with the antiferromagnetic unpaired electrons residing at the respective iron centres, and one 11-et state (S = 5) with all the single electrons being up-spin. The negligible energy difference between these two spin-states shows that the antiferromagnetic couplings for the two iron centres of the compound **3-6** are quite week, because the distance between the two iron ions across diamagnetic cyanidometal –NC-M^{II}-CN- in each compounds is more than 10 Å. Compared with the low-lying S = 0 and 5 spin-states, other intermediate-spin states are at least 29 kcal/mol higher in energy and thus they will not be discussed further in text.

The IR spectrum were calculated and collected in Table 3 to compare with the experimental values. Generally, the DFT calculated frequencies are close to the experimental values and the deviation is in the range of 10~29 cm^{-1}. The trends of calculated frequency shift are in good agreement with the experimental data, such as the frequencies of trinuclear complexes **3-6** are smaller than those of mononuclear complexes **1** and **2**, and the Ru-based complexes (**3** and **4**) c have larger frequencies than that of the Os-based complexes (**5** and **6**). A small deviation exists in the case of chloride- and bromide-coordinated complexes where DFT predicts the smaller frequencies in the chloride-coordinated complexes but experiment shows an inverse shift. This may be caused by the sensitive reflection of the frequency from the C≡N bonds for which DFT calculation obtains nearly the same C≡N bond lengths of chloride- and bromide-coordinated complexes in gas phase while the experiment obtains relatively longer C≡N bonds of bromide-coordinated complexes in crystal phase.

To investigate the spin-orbit coupling between high-spin iron centres, we calculated the effective exchange integrals J and g tensors as shown in Table 6. The absolute J values are smaller

than 0.1 cm^{-1}, which further shows that the antiferromagnetic interactions between two irons are very weak. The *g* values are within 2.02~2.05, very close to the corresponding *g* value of free electron indicating no spin-orbit coupling effect exists between high-spin Fe^{3+} ions.

Conclusions

In this work, two mononuclear cyanide precursors *cis*-$M(dppm)_2(CN)_2$ (M = Ru, **1**; M =Os, **2**) were prepared and used as diamagnetic cyanidometal bridge to synthesize four cyanide-bridged complexes *cis*-$M(dppm)_2(CN)_2(FeX_3)_2$ (M = Ru, X = Cl, **3**; M = Ru, X = Br, **4**; M = Os, X = Cl, **5**; M = Os, X = Br, **6**) with tri-nuclear V-shaped structure. Complexes **1-6** were all characterized by single-crystal X-ray diffraction, elemental analysis, IR and electronic absorption spectra. Combination of the crystal structure data, IR and electronic absorption spectra, it indicates the presence of some electron delocalization along Fe^{III}-NC-M^{II} arrays in complexes **3-6**. The theoretical calculations on the crystal structural data and IR spectroscopy, are good agreement with the experimental data. Furthermore, the investigation of magnetic properties of complexes **3-6** reveals that there exists only a very weak metal-metal interaction between distant Fe^{III} ions across the diamagnetic $NCM^{II}(dppm)_2CN$ bridge, which is also supported by theoretical calculations.

Acknowledgements

We acknowledge the financial support from 973 Program (2012CB821702 and 2014CB845603), the National Science Foundation of China (21173223 and 21233009).

Table 1. Crystallographic Data and Details of Structure Determination for Complexes **1-6.**

Complex	**1**·CH_2Cl_2	**2**·CH_2Cl_2	**3**·C_3H_7OH
Chemical formula	$C_{53}H_{46}Cl_2N_2P_4Ru$	$C_{53}H_{46}Cl_2N_2P_4Os$	$C_{55}H_{52}Cl_6Fe_2N_2OP_4Ru$
Formula weight	1006.77	1095.90	1306.34
Colour and Habit	yellow prism	yellow prism	red prism
Crystal Size / mm	0.870×0.172×0.100	0.391×0.206×0.158	0.713×0.247×0.072
T / K	123	123	123
Crystal system	triclinic	triclinic	triclinic
Space group	*P*-1	*P*-1	*P*-1
a / Å	11.113(3)	11.028(4)	11.440(4)
b /Å	11.793(2)	11.737(4)	13.303(5)
c / Å	20.606(5)	20.245(6)	20.957(9)
α / deg	77.458(7)	91.838(3)	83.618(12)
β / deg	74.385(8)	105.346(4)	78.271(12)
γ / deg	69.773(7)	109.564(2	65.726(11)
V / Å^3	2417.5(9)	2360.1(12)	2845.3(18)
Z	2	2	2
ρ_{calcd}(g/cm^3	1.383	1.542	1.525
)			
λ (Mo $K_α$, Å)	0.71073	0.71073	0.71073
μ(Mo $K_α$, mm^{-1})	0.605	2.989	1.199
Completeness	99.2%	98.0%	95.4%
F(000)	1032	1096	1324
h, *k*, *l*, range	-14≤*h*≤14, -15≤*k*≤15, -26≤*l*≤26	-14≤*h*≤14, -15≤*k*≤15, -26≤*l*≤26	-14≤*h*≤12, -17≤*k*≤17, -26≤*l*≤27
θ range / deg	2.05-27.52	2.01-27.45	2.07-27.41
Reflections measured	11052	10566	12364
R_{int}	0.0823	0.0460	0.0675
Params/restraints/Data(obs.)	577/24/8309	559/0/10394	665/33/10382
GOF	0.969	1.077	1.047
R_1, $_ωR_2$ (I>2σ(I))	0.0479, 0.1191	0.0387, 0.1019	0.0868, 0.2470
R_1, $_ωR_2$ (all data)	0.0595, 0.1440	0.0393, 0.1028	0.0977, 0.2654
Complex	**4**·2CH_3OH	**5**·CH_2Cl_2	**6**
Chemical formula	$C_{54}H_{52}Br_6Fe_2N_2O_2P_4Ru$	$C_{53}H_{46}Cl_8Fe_2N_2OsP_4$	$C_{52}H_{44}Br_6Fe_2N_2OsP_4$
Formula weight	1577.09	1420.30	1602.13
Colour and Habit	brown prism	red prism	brown prism
Crystal Size / mm	0.410×0.165×0.087	0.480×0.143×0.124	0.419×0.153×0.058
T / K	123	123	123
Crystal system	triclinic	triclinic	triclinic
Space group	*P*-1	*P*-1	*P*-1
a / Å	11.701(3)	11.400(3)	11.695(2)
b /Å	13.478(4)	13.291(4)	13.440(3)
c / Å	21.080(8)	21.017(6)	20.777(5)
α / deg	83.673(13)	83.848(11)	82.415(9)
β / deg	77.949(13)	77.910(10)	81.139(8)
γ / deg	65.687(9)	65.448(8)	65.160(6)
V / Å^3	2961.8(17)	2831.5(13)	2920.0(10)
Z	2	2	2
ρ_{calcd}(g/cm^3)	1.768	1.666	1.822
λ (Mo $K_α$, Å)	0.71073	0.71073	0.71073
μ (Mo $K_α$, mm^{-1})	4.931	3.272	6.910
Completeness	95.0%	96.0%	95.0%
F(000)	1544	1404	1536

h, k, l, range	-13≤h≤13, -14≤k≤16, -25≤l≤25	-14≤h≤14, -17≤k≤17, -26≤l≤27	-13≤h≤13, -15≤k≤15, -24≤l≤24
θ range / deg	2.33-25.00	2.03-27.52	2.05-25.00
Reflections measured	9897	12525	9760
R_{int}	0.0706	0.0832	0.0713
Params/restraints/Data(obs.)	714/155/8468	732/60/11040	604/18/8382
GOF	1.062	1.055	1.045
R_1, $_\omega R_2$ (I>2σ(I))	0.0817, 0.2200	0.0714, 0.2026	0.0865, 0.2256
R_1, $_\omega R_2$ (all data)	0.0897, 0.2310	0.0831, 0.2316	0.0939, 0.2382

Table 2. Selected Bond Lengths (Å) and Bond Angles (°) for Complexes **1-6.**

Complex	**1**	**2**		
M1-C51	2.035(4)	2.060(4)		
M1-C52	2.045(3)	2.058(4)		
M1-P1	2.339(1)	2.345(1)		
M1-P2	2.377(1)	2.371(1)		
M1-P3	2.348(1)	2.334(1)		
M1-P4	2.387(1)	2.363(1)		
C51≡N1	1.152(5)	1.137(6)		
C52≡N2	1.141(4)	1.143(6)		
C51-M1-C52	84.6(1)	84.4(2)		
N1≡C51-M1	176.3(3)	176.5(3)		
N2≡C52-M1	175.0(3)	177.0(4)		
Complex	**3**	**4**	**5**	**6**
M1-C51	1.988(7)	1.975(7)	2.016(9)	1.973(10)
M1-C52	1.992(7)	1.983(7)	2.004(9)	1.972(10)
M1-P1	2.368(2)	2.373(2)	2.364(2)	2.367(2)
M1-P2	2.400(2)	2.397(2)	2.405(2)	2.408(2)
M1-P3	2.356(2)	2.357 (2)	2.370(2)	2.379(2)
M1-P4	2.406(2)	2.407(2)	2.397(2)	2.408(2)
C51≡N1	1.156(9)	1.181(9)	1.130(12)	1.156(12)
C52≡N2	1.154(9)	1.168(9)	1.144(12)	1.157(13)
C51-M1-C52	87.9(3)	88.0(3)	87.4(3)	88.9(3)
N1≡C51-M1	174.3(6)	173.6(6)	175.2(8)	175.2(8)
N2≡C52-M1	177.2(6)	176.2(6)	177.5(8)	176.7(8)
C51≡N1-Fe1	166.4(6)	167.8(6)	164.6(8)	163.9(8)
C52≡N2-Fe2	173.3(6)	174.2(6)	171.5(9)	170.7(8)
Fe1-N1	1.958(6)	1.955(6)	1.961(8)	1.961(8)
Fe2-N2	1.956(6)	1.950(6)	1.950(9)	1.967(7)
Fe1-X1	2.158(3)	2.296(2)	2.162(3)	2.310(2)
Fe1-X2	2.167(3)	2.312(2)	2.176(3)	2.289(2)
Fe1-X3	2.175(2)	2.322(1)	2.178(3)	2.308(2)
Fe2-X4	2.202(3)	2.302(2)	2.170(3)	2.327(2)
Fe2-X5	2.168(3)	2.318(2)	2.199(3)	2.298(2)
Fe2-X6	2.170(3)	2.348(2)	2.180(3)	2.315(2)
$M^{II}\cdots Fe1^{III}$	5.04	5.06	5.04	5.02
$M^{II}\cdots Fe2^{III}$	5.09	5.09	5.09	5.07
$Fe^{III}\cdots Fe^{III}$	6.87	6.79	6.91	6.77
$Fe^{III}\cdots Fe^{III}$ (NC-M-CN)	10.20	10.21	10.21	10.19

Table 3. Comparison of Experimental and Theoretical Values of IR spectrum (KBr pellet, in cm^{-1}).

	exp		calc	
	ν_{CN1}	ν_{CN2}	ν_{CN1}	ν_{CN2}
1	2105	2091	2127	2120
2	2108	2088	2124	2112
3	2092	2062	2109	2083
4	2090	2059	2113	2088
5	2085	2048	2095	2061
6	2081	2042	2101	2069

Table 4. Electronic Absorption Spectral Data of Complexes **1-6**, $FeCl_3$ and $FeBr_3$ in CH_3CN solution at room temperature.

Complex	λ_{max}, nm (ε, $dm^3\ mol^{-1}\ cm^{-1}$)
1	325 (2042), 361(922)
2	318 (3213), 360 (824)
$FeCl_3$	209 (5422), 249 (8943), 322 (5092), 371 (5252)
$FeBr_3$	206 (9932), 230 (5817), 288 (7063), 328 (3617), 400 (3828), 478 (3922)
3	311 (12251), 358 (11229), 542 (2939)
4	390 (7551), 422 (7458), 464 (7128), 594 (2777)
5	301(11914), 359 (10768), 542 (3996), 664 (2691)
6	390 (8322), 420 (8195), 466 (7534), 610 (2943), 740 (1984)

Table 5. Related Energies of Different Spin States (S) of Complexes **3-6**, in kcal/mol.

Spin	**3**	**4**	**5**	**6**
0	0.0	0.0	0.0	0.0
1	92.4	106.7	92.2	86.8
2	77.7	116.3	77.8	71.9
3	62.8	61.3	64.7	43.7
4	31.5	50.9	31.9	29.0
5	0.0	0.0	0.0	0.0

Table 6. Computations of J and g Tensor for Complexes **3-6**.

	J (cm^{-1})	g
3	0.06	2.02

4	-0.07	2.05
5	0.03	2.02
6	0.06	2.05
$FeCl_3$		2.03
$FeBr_3$		2.06

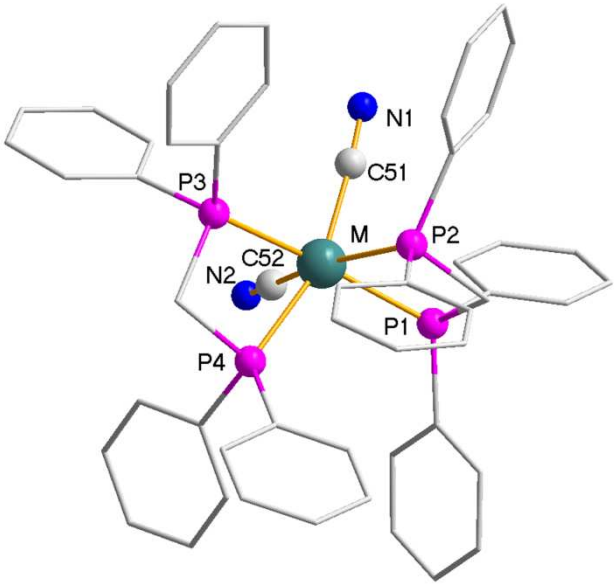

Figure 1. Molecular structure of *cis*-$M^{II}(dppm)_2(CN)_2$ [M = Ru, **1**; M = Os, **2**]. Hydrogen atoms and solvent molecules have been omitted for the sake of clarity.

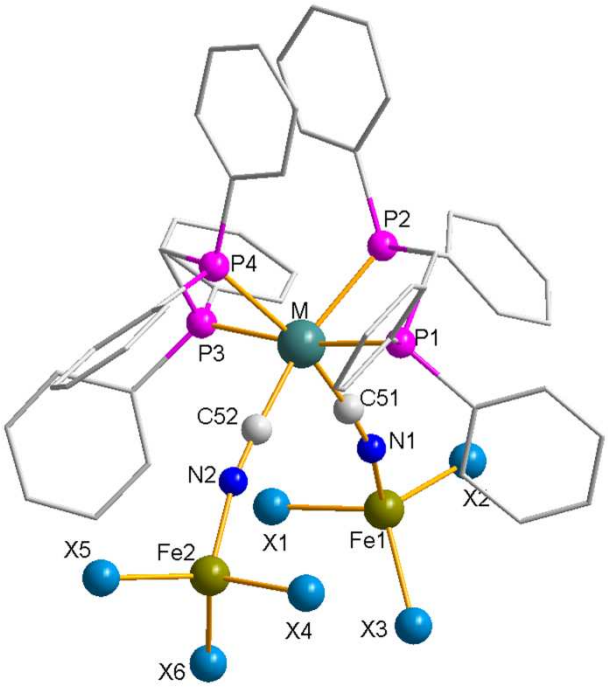

Figure 2. Molecular structures of *cis*-$M^{II}(dppm)_2(CN)_2(Fe^{III}X_3)_2$ [M = Ru, X = Cl, **3**; M = Ru, X = Br, **4**; M = Os, X = Cl, **5**; M = Os, X = Br, **6**]. Hydrogen atoms and solvent molecules have been omitted for the sake of clarity.

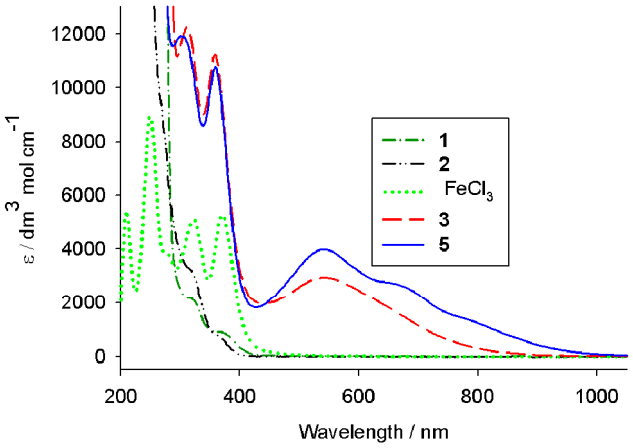

Figure 3. Electronic absorption spectra of complexes **1**, **2**, **3**, **5** and $FeCl_3$ measured CH_3CN solution at room temperature.

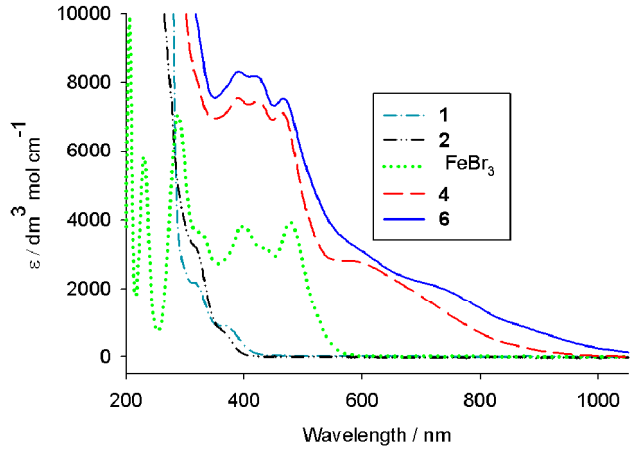

Figure 4. Electronic absorption spectra of complexes **1**, **2**, **4**, **6** and $FeBr_3$ measured CH_3CN solution at room temperature.

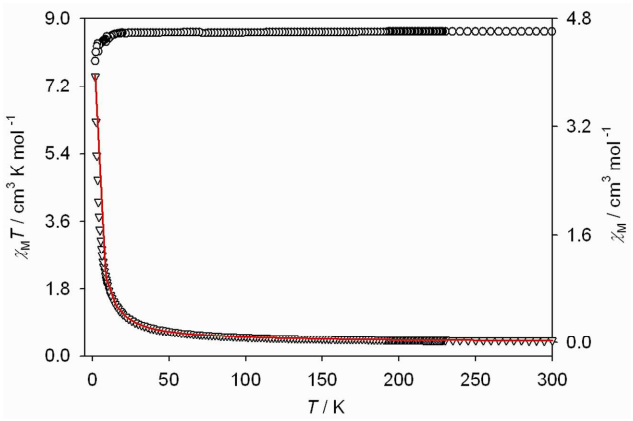

Figure 5. Magnetic behavior of complex **3** as measured in an applied field of 1000 Oe using a SQUID magnetometer. Fitting (red line) on χ_M vs T (star) and $\chi_M T$ vs T (circle) of complex **3** in polycrystalline sample.

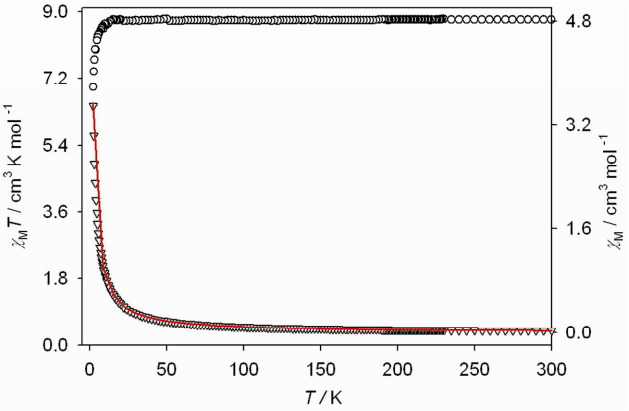

Figure 6. Magnetic behavior of complex **4** as measured in an applied field of 1000 Oe using a SQUID magnetometer. Fitting (red line) on χ_M vs T (star) and $\chi_M T$ vs T (circle) of complex **4** in polycrystalline sample.

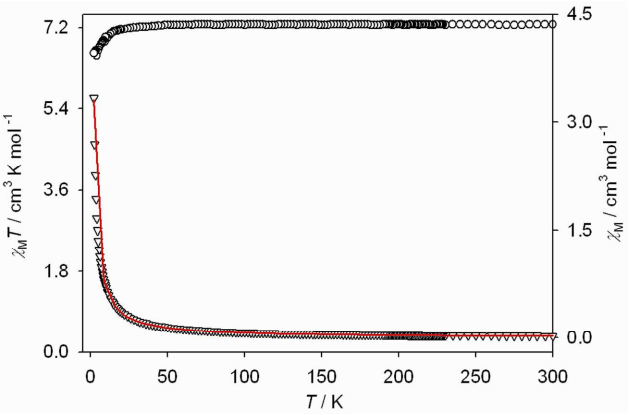

Figure 7. Magnetic behavior of complex **5** as measured in an applied field of 1000 Oe using a SQUID magnetometer. Fitting (red line) on χ_M vs T (star) and $\chi_M T$ vs T (circle) of complex **5** in polycrystalline sample.

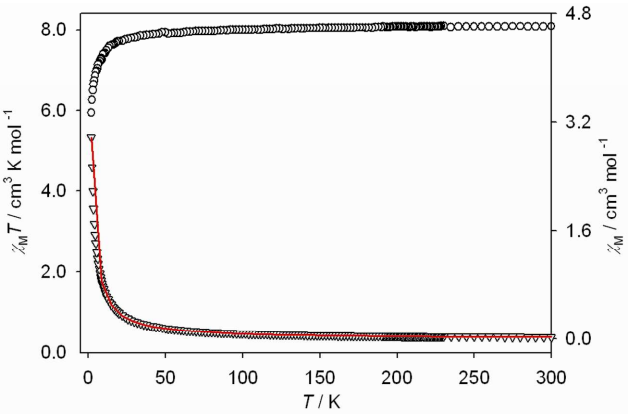

Figure 8. Magnetic behavior of complex **6** as measured in an applied field of 1000 Oe using a SQUID magnetometer. Fitting (red line) on χ_M vs T (star) and $\chi_M T$ vs T (circle) of complex **6** in polycrystalline sample.

Notes and references

[a] *State Key Laboratory of structure Chemistry, Fujian Institute of Research on Structure of Matter, Chinese Academy of Sciences, Fuzhou, 350002, China; E-mail: chunsen.li@fjirsm.ac.cn, tsheng@fjirsm.ac.cn.*
[b] *School of Chemistry and Chemical Engineering, University of Chinese Academy of Sciences, Beijing, 100049, China.*
[c] *Fujian Provincial Key Laboratory of Theoretical and Computational Chemistry, Xiamen, Fujian 361005, China.*

† Electronic Supplementary Information (ESI) available: [X-ray crystallographic data in CIF format for complexes **1-6**]. See DOI: 10.1039/b000000x/

‡ Footnotes should appear here. These might include comments relevant to but not central to the matter under discussion, limited experimental and spectral data, and crystallographic data.

1. J. F. Endicott and Y. J. Chen, *Coord. Chem. Rev.*, 2013, **257**, 1676; K. D. Demadis, C. M. Hartshorn and T. J. Meyer, *Chem. Rev.*, 2001, **101**, 2655; B. S. Brunschwig, C. Creutz and N. Sutin, *Chem. Soc. Rev.*, 2002, **31**, 168.
2. D. M. D'Alessandro and F. R. Keene, *Chem. Rev.*, 2006, **106**, 2270.
3. D. M. D'Alessandro and F. R. Keene, *Chem.-Eur. J.*, 2005, **11**, 3679.
4. T. Liu, D. P. Dong, S. Kanegawa, S. Kang, O. Sato, Y. Shiota, K. Yoshizawa, S. Hayami, S. Wu, C. He and C. Y. Duan, *Angew. Chem. Int. Ed.*, 2012, **51**, 4367; H. I. Karunadasa and J. R. Long, *Angew. Chem. Int. Ed.*, 2009, **48**, 738; C. P. Berlinguette, A. Dragulescu-Andrasi, A. Sieber, H. U. Gudel, C. Achim and K. R. Dunbar, *J. Am. Chem. Soc.*, 2005, **127**, 6766; S. Wang, J. L. Zuo, S. Gao, Y. Song, H. C. Zhou, Y. Z. Zhang and X. Z. You, *J. Am. Chem. Soc.*, 2004, **126**, 8900.
5. M. D. Ward, *Coord. Chem. Rev.*, 2006, **250**, 3128; J. Herrera, S. J. A. Pope, A. J. H. M. Meijer, T. L. Easun, H. Adams, W. Z. Alsindi, X.-Z. Sun, M. W. George, S. Faulkner and M. D. Ward, *J. Am. Chem. Soc.*, 2007, **129**, 11491; T. Lazarides, T. L. Easun, C. VeyneMarti, W. Z. Alsindi, M. W. George, N. Deppermann, C. A. Hunter, H. Adams and M. D. Ward, *J. Am. Chem. Soc.*, 2007, **129**, 4014.
6. S. Ohkoshi, H. Tokoro and K. Hashimoto, *Coord. Chem. Rev.*, 2005, **249**, 1830; S. Brossard, F. Volatron, L. Lisnard, M. A. Arrio, L. Catala, C. Mathoniere, T. Mallah, C. C. D. Moulin, A. Rogalev, A. Smekhova and P. Sainctavit, *J. Am. Chem. Soc.*, 2012, **134**, 222.
7. H. Oshio, H. Onodera and T. Ito, *Chem.-Eur. J.*, 2003, **9**, 3946; T. Hozumi, K. Hashimoto and S. Ohkoshi, *J. Am. Chem. Soc.*, 2005, **127**, 3864; C. F. Wang, W. Liu, Y. Song, X. H. Zhou, J. L. Zuo and X. Z. You, *Eur. J. Inorg. Chem.*, 2008, 717; J. Yang, D. Seneviratne, G. Arbatin, A. M. Andersson and J. C. Curtis, *J. Am. Chem. Soc.*, 1997, **119**, 5329.
8. M. B. Robin, *Inorg. Chem.*, 1962, **1**, 337.
9. X. Ma, S. M. Hu, C. H. Tan, Y. H. Wen, Q. L. Zhu, C. J. Shen, T. L. Sheng and X. T. Wu, *Dalton Trans.*, 2012, **41**, 12163; X. Ma, S. M. Hu, C. H. Tan, Y. F. Zhang, X. D. Zhang, T. L. Sheng and X. T. Wu, *Inorg. Chem.*, 2013, **52**, 11343.
10. X. Ma, C. S. Lin, S. M. Hu, C. H. Tan, Y. H. Wen, T. L. Sheng and X. T. Wu, *Chem.-Eur. J.*, 2014, **20**, 7025; Y. Wang, X. Ma, S. M. Hu, Z. Z. Xue, Y. H. Wen, X. Q. Zhu, T. L. Sheng and X. T. Wu, *Dalton Trans.*, 2014, **43**, 17453.
11. B. P. Sullivan and T. J. Meyer, *Inorg. Chem.*, 1982, **21**, 1037.
12. B. Chaudret, G. Commenges and R. Poilblanc, *J. Chem. Soc., Dalton Trans.*, 1984, **0**, 1635.
13. J. Chatt and R. G. Hayter, *J. Chem. Soc.*, 1961, **0**, 896.
14. G. M. Sheldrick, *SHELXL-97*, **1997**, University of Göttingen, Germany
15. C. T. Lee, W. T. Yang and R. G. Parr, *Phys. Rev. B*, 1988, **37**, 785; A. D. Becke, *J. Chem. Phys.*, 1993, **98**, 5648.
16. M. J. Frisch, G. W. Trucks, H. B. Schlegel, G. E. Scuseria, M. A. Robb, J. R. Cheeseman, J. A. Montgomery, T. Vreven, K. N. Kudin, J. C. Burant, J. M. Millam, S. S. Iyengar, J. Tomasi, V. Barone, B. Mennucci, M. Cossi, G. Scalmani, N. Rega, G. A. Petersson, H. Nakatsuji, M. Hada, M. Ehara, K. Toyota, R. Fukuda, J. Hasegawa, M. Ishida, T. Nakajima, Y. Honda, O. Kitao, H. Nakai, M. Klene, X. Li, J. E. Knox, H. P. Hratchian, J. B. Cross, C. Adamo, J. Jaramillo, R. Gomperts, R. E. Stratmann, O. Yazyev, A. J. Austin, R. Cammi, C. Pomelli, J. W. Ochterski, P. Y. Ayala, K. Morokuma, G. A. Voth, P. Salvador, J. J. Dannenberg, V. G. Zakrzewski,

S. Dapprich, A. D. Daniels, M. C. Strain, O. Farkas, D. K. Malick, A. D. Rabuck, K. Raghavachari, J. B. Foresman, J. V. Ortiz, Q. Cui, G. Baboul, S. Clifford, J. Cioslowski, B. B. Stefanov, G. Liu, A. Liashenko, P. Piskorz, I. Komaromi, R. L. Martin, D. J. Fox, T. Keith, M. A. Al-Laham, C. Y. Peng, A. Nanayakkara, M. Challacombe, P. M. W. Gill, B. Johnson, W. Chen, M. W. Wong, C. Gonzalez and J. A. Pople, *Gaussian 03, Revision D.01*, **2004**, Gaussian, Inc., Wallingford CT.

17. M. W. Wong, *Chem. Phys. Lett.*, 1996, **256**, 391.

18. F. Neese, *Wiley Interdiscip. Rev.-Comput. Mol. Sci.*, 2012, **2**, 73.

19. F. Weigend and R. Ahlrichs, *Phys. Chem. Chem. Phys.*, 2005, **7**, 3297.

20. F. Neese, *J. Chem. Phys.*, 2005, **122**, 13.

21. T. Soda, Y. Kitagawa, T. Onishi, Y. Takano, Y. Shigeta, H. Nagao, Y. Yoshioka and K. Yamaguchi, *Chem. Phys. Lett.*, 2000, **319**, 223.

22. W. D. Jones and W. P. Kosar, *Organometallics*, 1986, **5**, 1823.

23. K. M. Anderson and A. G. Orpen, *Chem. Commun.*, 2001, 2682.

24. B. J. Coe, T. J. Meyer and P. S. White, *Inorg. Chem.*, 1995, **34**, 3600; C. A. Bignozzi, R. Argazzi, J. R. Schoonover, K. C. Gordon, R. B. Dyer and F. Scandola, *Inorg. Chem.*, 1992, **31**, 5260.

25. W. Kaim and B. Sarkar, *Coord. Chem. Rev.*, 2013, **257**, 1650; D. M. D'Alessandro, A. C. Topley, M. S. Davies and F. R. Keene, *Chem.-Eur. J.*, 2006, **12**, 4873; D. M. D'Alessandro, P. H. Dinolfo, M. S. Davies, J. T. Hupp and F. R. Keene, *Inorg. Chem.*, 2006, **45**, 3261.

26. M. Srnec, J. Chalupský, M. Fojta, L. Zendlová, L. k. Havran, M. Hocek, M. r. Kývala and L. r. Rulíšek, *J. Am. Chem. Soc*, 2008, **130**, 10947; E. M. J. Johansson, M. Odelius, S. Plogmaker, M. Gorgoi, S. Svensson, H. Siegbahn and H. Rensmo, *J. Phys. Chem. C*, 2010, **114**, 10314; L. Rulíšek, *J. Phys. Chem. C*, 2013, **117**, 16871.

27. G. Rogez, A. Marvilliers, E. Riviere, J. P. Audiere, F. Lloret, F. Varret, A. Goujon, N. Mendenez, J. J. Girerd and T. Mallah, *Angew. Chem. Int. Ed.*, 2000, **39**, 2885.

Synthesis, Crystal Structure and MMCT of New Cyanide-bridged Complexes *cis*-$M^{II}(dppm)_2(CN)_2(Fe^{III}X_3)_2$ (M = Ru，Os)

Yong Wang,[a, b] Jinshuai Song,[a] Xiao Ma,[a] Zhenzhen Xue,[a, b] Shengmin Hu,[a] Ruibiao Fu,[a] Chunsen Li,*[a] Tianlu Sheng*[a] and Xintao Wu[a]

[a]*State Key Laboratory of Structure Chemistry, Fujian Institute of Research on the Structure of Matter, Chinese Academy of Sciences, Fuzhou, 350002, China. E-mail:* chunsen.li@fjirsm.ac.cn, tsheng@fjirsm.ac.cn.

[b]*School of Chemistry and Chemical Engineering, University of Chinese Academy of Sciences, Beijing, 100049, China.*

Two cyanide precursors *cis*-$M^{II}(dppm)_2(CN)_2$ (M = Ru, **1**; Os, **2**) and four new cyanide-bridged complexes *cis*-$M^{II}(dppm)_2(CN)_2(Fe^{III}X_3)_2$ (M = Ru, X = Cl, **3**; M = Ru, X = Br, **4**; M = Os, X = Cl, **5**; M = Os, X = Br, **6**) were synthesized and investigated. The investigations reveal the presence of MMCT from central M^{II} to terminal Fe^{III} in **3-6**. The magnetic properties of complexes **3-6** indicate the very weak metal-metal interaction.